forests

Article

Individual-Tree Stem Volume Modeling Using Handheld LiDAR and UAV-SfM Photogrammetry in a Mediterranean Mixed Forest

Chamodi Tharuni Mahanama Dissanayake *, Frederico Tupinambá-Simões, Aitor Vázquez-Veloso and Felipe Bravo

SMART Ecosystems Group, Departamento de Producción Vegetal y Recursos Forestales, Instituto Universitario de Investigación en Gestión Forestal Sostenible (iuFOR), ETS Ingenierías Agrarias, Universidad de Valladolid, 34004 Palencia, Spain; frederico.tupinamba@uva.es (F.T.-S.); aitor.vazquez.veloso@uva.es (A.V.-V.); felipe.bravo@uva.es (F.B.)

* Correspondence: chamodi.mahanama@uva.es

Abstract

Integrating ground-based and aerial remote sensing for individual tree-level stem volume modeling remains underexplored in Mediterranean mixed forests, despite the growing need for cost-effective, automated forest inventory approaches. This study evaluated the combined use of Handheld Laser Scanning (HLS) and Unmanned Aerial Vehicle (UAV)-based Structure from Motion (SfM) photogrammetry for individual-tree stem volume modeling in a mixed stand in Castilla y León, Spain, dominated by *Pinus halepensis*, *Pinus pinea*, *Quercus faginea*, and *Cupressus sempervirens*. Two open-source HLS processing tools; the Forest Structural Complexity Tool (FSCT) and 3D Forest Inventory (3DFin), were compared for individual tree attribute extraction, with FSCT outperforming 3DFin across all species. Reference stem volumes were derived by applying species-specific Spanish National Forest Inventory (SNFI) allometric equations to FSCT-extracted diameter and height values. Random Forest models were then built using UAV-SfM crown metrics as predictors, testing two image overlap configurations: 80 × 80 F (80% front and side overlap) and 80 × 60 CF (80% front, 60% side, cross-flight). The 80 × 80 F configuration produced the best-performing model (R^2 = 0.730), with 80 × 60 CF achieving comparable accuracy (R^2 = 0.688), results confirmed by spatially independent leave-one-plot-out cross-validation (LOPO-CV R^2 = 0.627 and 0.613, respectively). These results show that combining HLS and UAV-SfM through a predominantly open-source workflow offers a viable, reproducible approach to stem volume modeling in structurally complex Mediterranean mixed forests.

Keywords: Handheld Laser Scanner (HLS); Structure from Motion (SfM); random forest; forest inventory; Unmanned Aerial Vehicle (UAV)

Check for updates

Academic Editor: Mark Vanderwel

Received: 8 July 2026
Revised: 3 August 2026
Accepted: 7 August 2026
Published: 9 August 2026

1. Introduction

Mediterranean forests represent a unique ecoregion characterized by a dry, warm climate with pronounced summer drought, placing vegetation under recurring physiological stress [1,2]. These ecosystems are ecologically complex and multifunctional, providing a wide range of provisioning and regulating services [3,4]. Mixed Mediterranean stands often feature structurally heterogeneous species compositions, including multi-stemmed broadleaves such as *Quercus faginea* Lam., that increase both ecological value and inventory complexity [5]. Accurate forest measurement is therefore a critical input for the decision-making process underpinning sustainable and multifunctional forest management [6].

Forest inventories serve as the primary tool for providing the needed information to support sustainable and multifunctional forest management, ensuring the continued provision of ecological services, assessing forest structure, and quantifying different forest resources [7,8]. Traditional methods rely on on-ground surveys, where foresters record tree species and measure tree attributes such as height (*h*), diameter at breast height (*dbh*), and crown dimensions. These field measurements are subsequently used in allometric equations to estimate volume, biomass, and other tree and stand-level variables [9–13]. While accurate, these techniques are labour-intensive, time-consuming, and prone to human error, limiting their applicability at large spatial scales and in structurally complex stands [14].

Stem volume at the individual-tree level is a key variable in forest inventory, typically estimated using allometric equations applied to field-measured *dbh* and *h*. In Spain, species-specific allometric equations provided by the Spanish National Forest Inventory (SNFI) represent the operational standard [15]. However, these equations were developed several decades ago using tree measurement data that may not fully reflect contemporary stand conditions. Changes in growth rates driven by climate change and shifting management practices, including thinning schedules and rotation lengths, can cause systematic deviations between predicted and actual volumes when historical allometric parameters are applied to present-day trees [16]. Despite these known limitations, SNFI equations remain the operational standard in Spanish forest inventory practice and are therefore adopted here to ensure comparability with national forest assessments. In the present study, anomalous volume estimates for *Pinus halepensis* Mill. were found by using its regional parameterization. Although species- and region-specific taper equations are also available [17–19], they are not the actual benchmark. Here, we apply the method used by forest practitioners in real-world situations in Spain.

Remote sensing technologies, particularly Light Detection and Ranging (LiDAR) and Structure from Motion (SfM) photogrammetry, have substantially advanced stem volume modeling and estimation [20,21]. Among ground-based LiDAR systems, Handheld Laser Scanners (HLS) have emerged as a practical alternative to static Terrestrial Laser Scanning (TLS) [22], offering unlimited scan positions, high within-plot mobility, and time efficiency. In fact, it was reported to be 4.7 times faster than multi-scan TLS [23,24] while delivering accurate estimates of tree detection, *dbh*, and *h* [7,25,26]. However, HLS is inherently limited to plot-level data collection and does not scale efficiently to large forest areas without complementary aerial data sources.

UAV-based aerial imagery processed through SfM photogrammetry addresses this scaling limitation by enabling cost-effective, high-resolution 3D reconstruction of forest canopies across entire stands [27,28]. UAV-SfM point clouds have been shown to reliably capture crown-level structural attributes, including tree height and crown geometry, that serve as effective predictors of stem volume [29–32]. Image overlap configuration is a critical factor in UAV-SfM data quality: front and side overlaps between 60% and 80% are standard in forest inventory applications, with higher overlap values generally improving 3D reconstruction accuracy [27,33,34], while [35] reported that >90% overlap might be undesirable considering the flight time and transects increment. The integration of HLS and UAV-SfM, therefore, offers a compelling framework; HLS provides accurate ground-level tree attributes from which reference volumes can be derived, and UAV-SfM captures the crown-level structural information needed to extend predictions across entire forest stands. Recent work integrating ground-based personal laser scanning with UAV-based sensing has demonstrated promising accuracy for stem volume estimation at individual tree, plot, and stand levels in structurally simple temperate coniferous plantations [36]; however, such approaches have not yet been evaluated in structurally complex Mediterranean mixed forests, nor using predominantly open-source processing tools applicable to practitioners with limited budgets.

This study addresses that gap by (i) evaluating and comparing the performance of two open-source HLS processing tools, FSCT and 3DFin plugin (via CloudCompare), for extracting individual tree attributes; (ii) evaluating the reliability of FSCT-derived tree attributes as a functional substitute for field measurements in SNFI-based stem volume calculations; (iii) assessing the effect of UAV image overlap configurations on model accuracy, and (iv) developing Random Forest (RF) predictive models for individual-tree stem volume using SNFI-based reference volumes and UAV-SfM crown metrics as predictors.

To our knowledge, this is one of the first studies to systematically combine HLS and UAV-SfM photogrammetry for single-tree stem volume prediction in a Mediterranean mixed forest, using a predominantly open-source processing chain calibrated against national forest inventory standards. While previous work has demonstrated the individual value of each technology, the integration of ground-level structural attributes derived from HLS with canopy-level metrics from UAV-SfM, and the use of SNFI allometric equations as the reference volume standard represents a methodological contribution with direct operational relevance for Spanish forest inventory practice. The workflow proposed here is designed to be reproducible, cost-effective, and adaptable to other forest types where national allometric standards are available.

2. Methodology

2.1. Study Area

The study was conducted in a 30-hectare mixed forest stand near Ampudia, in Castilla y León region in Spain (41°51′54.44″ N, 4°46′21.69″ W) (Figures 1 and 2). The region has a continental Mediterranean climate classified as Csa (hot-summer Mediterranean) under the Köppen–Geiger system, characterized by hot, dry summers and cold winters, with a mean annual temperature of 11.9 °C and mean annual precipitation of approximately 491 mm [37]. The forest stand mainly comprises five tree species from three genera: *Pinus halepensis* Mill., *Pinus pinea* L., and *Cupressus sempervirens* L., planted for restoration purposes, along with the natural regeneration of *Quercus faginea* Lam. and some scattered *Quercus ilex* L. individuals (although no *Q. ilex* individuals were recorded in our sampling plots).

Figure 1. (**a**) Representative view of the Mediterranean mixed forest stand near Ampudia, Palencia, Spain; (**b**) field data collection using the ZEB-Horizon HLS scanner within one of the nine circular sample plots.

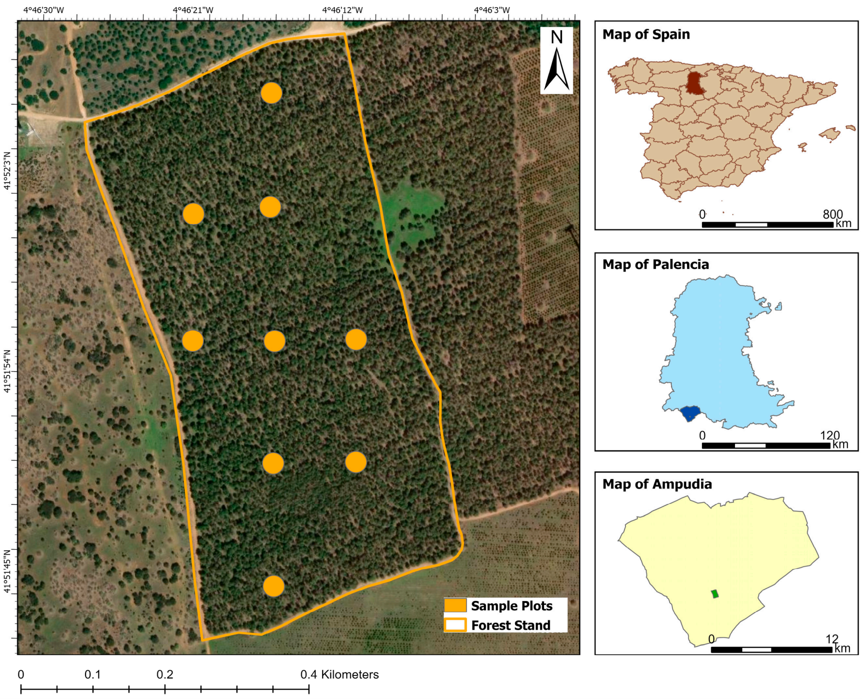

Figure 2. Study area map showing the 30-hectare forest stand and the nine circular sample plots.

2.2. Ground Data Collection and Analysis

The overall methodological workflow comprises three integrated components: ground-based data collection and HLS processing (Section 2.2), UAV imagery acquisition and processing (Section 2.3), and RF model development (Section 2.4), together forming a complete pipeline from field data acquisition to single-tree stem volume prediction.

Data were collected using three complementary methods: traditional field inventory and HLS applied across nine sampling plots, and UAV-based aerial imaging applied to the whole stand.

2.2.1. Field Inventory and Preliminary Data Processing

Nine circular sample plots of 12 m radius were established, with an additional 3 m buffer to minimize edge effects. In each plot, trees with *dbh* < 7 cm were excluded from the analysis. Geographic coordinates of five reference points per plot (marked in red points in Figure 3: center, North, East, South, West points) were recorded using a Topcon GNSS receiver (Topcon Corporation, Tokyo, Japan) in post-processed mode to support spatial referencing of HLS data. Reference points were marked in the field using painted wooden sticks placed at cleared locations to ensure unobstructed GNSS signal reception. Post-processed kinematic (PPK) positioning was used to achieve sub-decimetre horizontal accuracy, with observation sessions of approximately 10 min per point to ensure sufficient satellite coverage under partial canopy. Under dense canopy, signal multipath and reduced satellite visibility were mitigated by selecting points at canopy gaps where possible.

For the traditional inventory, the tree species, diameter at breast height (*dbh*), and total height (*h*) were recorded using standard forest inventory tools. Tree *dbh* was measured with a diameter caliper (±1 mm precision) as the mean of two perpendicular readings at breast height (1.3 m), and *h* was measured with a Vertex Laser Geo hypsometer (±0.1 m precision). In total, 157 trees were measured across all plots (Table 1) under leaf-on conditions to ensure consistency with HLS and UAV data acquisition. For subsequent analyses, species were grouped by genus: pinewoods (*P. halepensis* and *P. pinea*), oak (*Q. faginea*), and cypress (*C. sempervirens*).

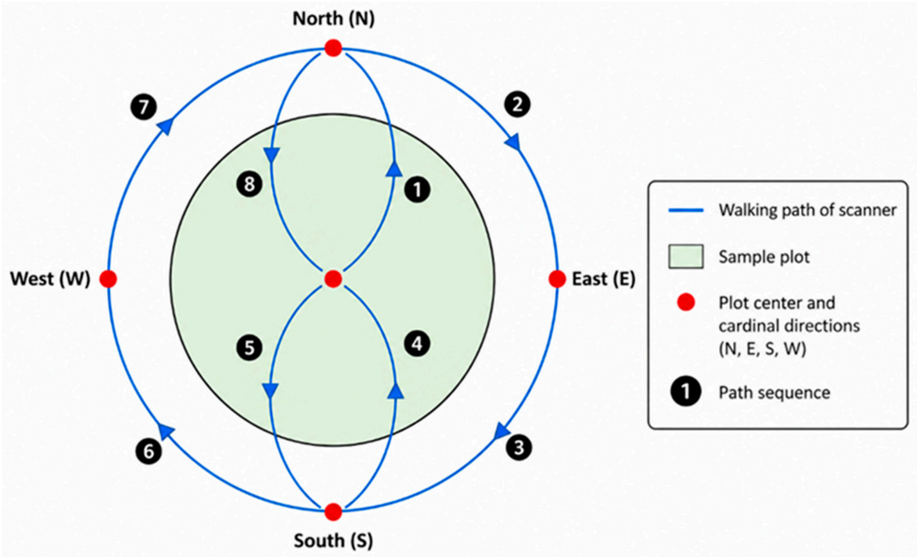

Figure 3. Walking path for HLS data collection inside each circular plot, following two closing loops from the center outward.

Table 1. Summary of traditional inventory by tree species and their main attributes, including number of trees (n), diameter at breast height (*dbh*), total height (*h*) and the corresponding mean (mean), maximum (max), and minimum (min) values. Pinewoods include both *Pinus halepensis* and *P. pinea*.

Tree Species	n	***dbh* (cm)**			***h* (m)**		
		Mean	**Max**	**Min**	**Mean**	**Max**	**Min**
Pinewoods	93	29.15	44.95	15.85	11.0	16.3	6.9
i. P. halepensis	55	31.37	44.95	18.1	12.8	16.3	9.5
ii. P. pinea	38	26.92	40.85	15.85	9.2	12.4	6.9
Oak (*Q. faginea*)	34	10.77	19.45	7.00	5.8	8.9	3.4
Cypress (*C. sempervirens*)	30	16.05	30.60	7.00	8.3	11.4	5.1

2.2.2. HLS Data Collection and Analysis

HLS data was acquired using a ZEB-HORIZON LiDAR Handheld Laser Scanner (GeoSLAM Ltd., Nottingham, UK) on each plot. The scanner captures 300,000 points per second using SLAM technology, allowing continuous data acquisition while moving through the plot. Scans were conducted under sunny, low-wind conditions. Each plot was scanned following two consistent closing loops as recommended on previous studies [25]; moving from the plot center toward the north and through the boundary back south to cover one half, then repeating for the other half with additional passes to ensure complete stem coverage from multiple angles (Figure 3). Each scan required approximately 15 min per plot.

HLS data were initially recorded in the proprietary GeoSLAM format (*.geoslam*) and converted to the widely supported *.las* format using FARO Connect GeoSLAM Hub (version 2025.0.0) [38]. Ground Control Points (GCPs) were georeferenced using Magnet Tools software (version 9.0) [39] to align point clouds spatially. Point clouds were then clipped to individual plot boundaries in R (version 4.4.1) [40] for further analysis.

The processed point clouds were analyzed using two open-source tools to extract individual tree attributes (tree position, *dbh* and *h*) namely the Forest Structural Complexity Tool (FSCT) [41] and the 3DFin plugin [42] within CloudCompare (version 2.13.2; [43]. FSCT is designed to automatically derive plot and tree-level structural metrics through semantic segmentation of point cloud data, while 3DFin performs automated forest inventories from terrestrial point clouds via tree individualization. Tree attributes extracted from both tools were compared against field inventory measurements to evaluate accuracy and to select the most suitable tool for subsequent stem volume calculation based on SNFI equations (Figure 4).

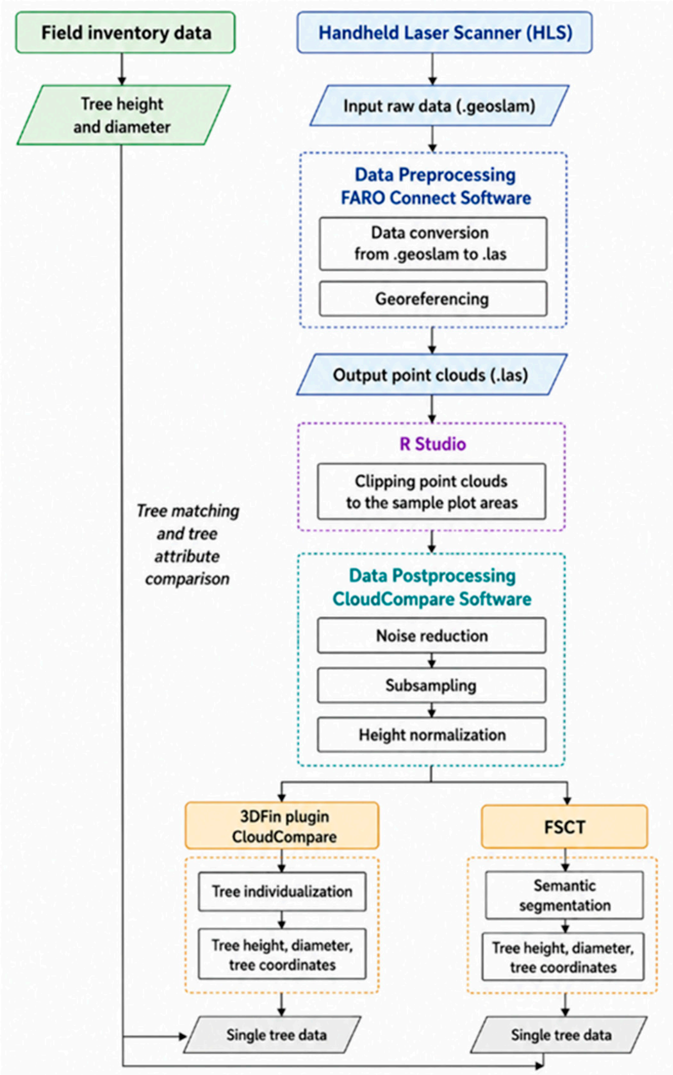

Figure 4. Flowchart of the HLS data processing workflow from raw point cloud to individual tree attribute extraction.

2.2.3. Stem Volume Calculation and Cross Validation

From the field-measured tree *dbh* and *h*, volume over bark was calculated using species-specific allometric equations from the SNFI [44]. For the target species, the same equation, but with different coefficients, was applied:

$$vcc = p \cdot dbh^{q} \cdot h^{r}$$

where *vcc* is the tree volume over bark (dm^3), *dbh* is the diameter at breast height (mm), *h* is total height (m), and *p*, *q*, and *r* represent specific equation parameters for each province, species, and tree quality (Table 2). Regarding tree quality, the classification scale ranges from 1 (straight, healthy dominant tree) to 6 (dead tree without signs of rot). However, the SNFI database does not cover all classes, frequently utilizing class 2 (healthy, vigorous tree with potential minor structural defects) as the default category [44].

Table 2. SNFI allometric parameters (*p*,*q*,*r*) used to estimate tree volume over bark according to province, tree species, and tree quality [44].

Province	Species	Tree Quality	*p*	*q*	*r*
Palencia	*P. halepensis*	2	0.0049296	2.0172500	−0.5889300
Burgos	*P. halepensis*	2	0.0010414	1.8585300	0.8476000
Palencia	*P. pinea*	2	0.0014257	1.7667300	0.9888200
Palencia	*Q. faginea*	2	0.0952676	1.2339900	0.1190100
Palencia	*C. sempervirens*	2	0.0014257	1.7667300	0.9888200

For *P. halepensis*, the standard SNFI coefficients for the Palencia province produced volumes substantially lower than expected given the field-measured *dbh* and *h* values, suggesting potential regional parameterization bias (Figure 5). This deviation likely reflects the fact that the Palencia parameterization was derived from a sample population with different structural characteristics; potentially younger or more suppressed trees than those present in the study stand, which was subject to restoration planting and subsequent thinning treatments. Following the SNFI methodology, the coefficients of the nearest geographically appropriate zone (Burgos) were therefore adopted for this species for further analysis. Additionally, *P. pinea* and *C. sempervirens* share the same parameters, reflecting standard SNFI practice for species with insufficient data for independent equation derivation, where a structurally similar conifer is used as a surrogate.

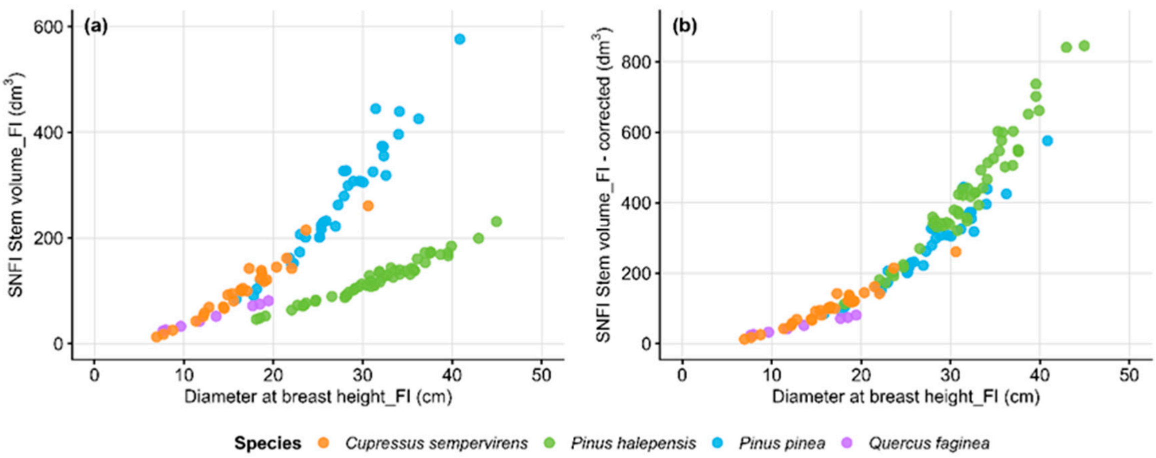

Figure 5. Observed deviation of *P. halepensis* stem volumes (**a**) with regional coefficients (**b**) corrected coefficients for *P. halepensis* from the nearest area.

Moreover, after selecting the best tool for tree attribute extractions from HLS data (in our case, it was FSCT), stem volume was calculated following the same SNFI allometric equation method above. Then, these independently derived volume sets (from FI and HLS-FSCT) were used to assess whether LiDAR-derived attributes could reproduce the volumes obtained through conventional field-based methods, which is a critical step toward validating automated forest inventory in Spanish Mediterranean stands where SNFI equations represent the operational standard.

2.3. UAV Imagery Acquisition and Processing

A DJI Mavic 3 Enterprise UAV (DJI Enterprise, Shenzhen, China) equipped with a 20 MP 4/3 CMOS RGB camera and mechanical shutter was used to capture aerial images of the entire forest stand. Two flight configurations (Figure 6) were tested:

- Flight 1 (80 × 80 F): Nadir-facing camera, 80% front and 80% side overlap, 245° flight angle (Figure 6a).
- Flight 2 (80 × 60 CF): Oblique camera angle (45° tilt), 80% front and 60% side overlap, cross-flight patterns at 245° and 225° angles (Figure 6b,c).

Figure 6. Drone routes; (**a**) 80% front and side overlap flight with 245° angle (80 × 80 F), (**b**) 80% front and 60% side overlap cross flights (80 × 60 CF) with 245° and (**c**) 225° angles.

Both missions were flown at 70 m altitude and 10 m/s under clear sky conditions. The 70 m flight altitude was selected to balance spatial resolution—yielding a ground sampling distance (GSD) of approximately 1.88 cm per pixel—with adequate canopy coverage, consistent with recommendations for forest inventory UAV applications [27,45]. Ground Control Points (GCPs) were established in canopy gaps and recorded using a Topcon Hiper SR GNSS receiver [39] to ensure accurate georeferencing. Approximately 1059 images were collected from 80 × 80 F and 1113 from 80 × 60 CF.

UAV images from both flight configurations (80 × 80 F and 80 × 60 CF) were processed independently using WebODM [46], an open-source photogrammetry platform based on OpenDroneMap, to generate dense 3D point clouds via SfM. GCPs were used as georeferencing targets. The resulting point clouds were clipped to the nine sample plots using an extended radius of 15 m (the original 12 m plot radius plus a 3 m outer buffer) to retain crown points of trees located near the plot boundary and minimise edge effects on crown metric extraction.

Point cloud processing was performed in R using the *lidR* package [47,48]. The workflow included (i) ground point classification using the Progressive Morphological Filter (PMF) [49]; applied with four progressive steps: window sizes of 3, 6, 9, and 12 m, and corresponding height thresholds of 0.10, 0.57, 1.03, and 1.50 m, as implemented in the *lidR* package [47,48]; (ii) height normalization using a k-nearest neighbour inverse-distance weighting (knnidw) spatial interpolation; (iii) generation of Canopy Height Models (CHM) via the point-to-raster algorithm; and (iv) individual tree top detection using a Local Maximum Filter (LMF). For individual tree segmentation, the CHM-based Voronoi tessellation algorithm [50] was applied, as it has demonstrated reliable crown delineation performance in mixed forest stands with overlapping canopies, consistent with the structural conditions of the present study.

Once the trees were segmented individually, tree tops and crown polygons were created using the *lidR* R package. Crown-level metrics were then extracted using the *lidRmetrics* package [51]. These metrics formed the basis of the predictive models for tree volume. The full processing workflow is illustrated in Figure 7.

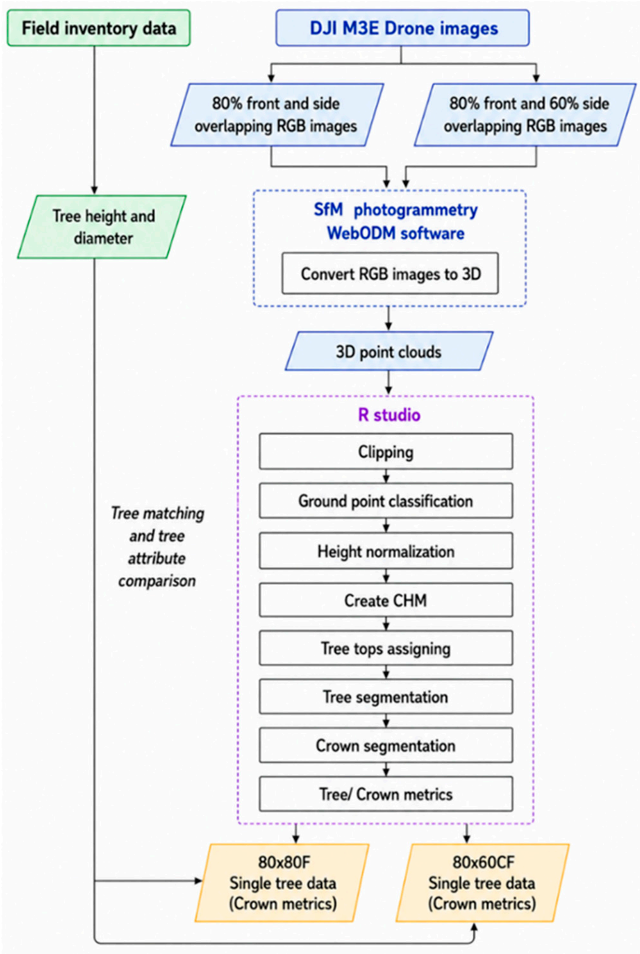

Figure 7. Flowchart of the UAV-SfM data processing workflow from drone image acquisition to crown metric extraction.

To enable reliable attribution of UAV-SfM crown metrics to their corresponding HLS-derived tree volumes, individual trees identified in the HLS-FSCT algorithm were spatially matched to tree tops delineated from the UAV-SfM data using QGIS (version 3.44) [52]. Both datasets, HLS-FSCT tree stem positions and UAV-SfM tree top coordinates, were loaded as separate vector layers within the same georeferenced coordinate system (EPSG: 25830-ETRS 89/UTM zone 30N) and visually inspected for spatial correspondence. All tree matching was performed manually through visual overlay, to ensure reliable one-to-one attribution in a structurally complex stand where automated nearest-neighbour approaches would be prone to misattribution. In ambiguous cases where two or more candidates fell within close proximity, particularly in areas of high tree density and overlapping crowns, field-measured *dbh* and *h* values were used as additional confirmation criteria. The trees with a confident match between both data sources, and for which complete UAV-SfM crown metrics could be extracted, were retained for model development.

2.4. Individual Stem Volume Model Development

Prior to modeling, each dataset was independently screened for variable distributions, outliers (using interquartile range thresholds), and missing values arising from incomplete crown segmentation. Both raw and log-transformed versions of all variables were examined.

Variable selection proceeded in two stages. First, crown metrics with an absolute Pearson correlation with stem volume below $|r| = 0.40$ were removed as uninformative predictors. Second, among the remaining candidates, where inter-variable correlations exceeded |r| = 0.70, the variable with the lower individual correlation to stem volume was excluded. This process was applied iteratively until no strongly correlated predictor pairs remained. RF [53] was selected as the modeling algorithm due to its strong performance in ecological modeling contexts with limited sample sizes. Two different models were developed separately for the 80 × 80 F and 80 × 60 CF UAV-flight configurations. The dependent variable was the tree volume over bark previously calculated from SNFI allometric equations applied to FSCT-derived *dbh* and *h* values. Independent variables consisted of UAV-SfM selected crown metrics extracted using the *lidRmetrics* package [51]. These RF models were implemented using the *randomForest* package [54] in R [40], with all hyperparameters retained at their default values (ntree = 500; mtry = 2 for the 80 × 80 F model and mtry = 1 for the 80 × 60 CF model). For each configuration, the dataset was randomly partitioned into training (70%) and testing (30%) subsets using the *caret* package [55] with a fixed random seed (set.seed(123)) to ensure reproducibility. Model performance on the test subset was evaluated using R^2 and RMSE. Additionally, leave-one-plot-out cross-validation (LOPO-CV) was performed to provide a spatially independent assessment of model generalizability, in which each of the nine sampling plots was sequentially withheld as an independent test set while the model was trained on trees from the remaining eight plots.

3. Results

3.1. HLS LiDAR and UAV-SfM Performance

HLS LiDAR data were processed under two different algorithms already detailed, FSCT and 3DFin, and compared against traditional field inventory to evaluate bias on tree detection and size (*dbh* and *h*).

Tree detection rates varied considerably between species and tools (Table 3). Both tools performed well for pinewoods and cypress, but oak detection was markedly lower. Regarding the algorithms used, differences were found in cypress and oak detection among them, highlighting that oak detection remained challenging for both tools.

Table 3. Tree detection by FSCT and 3DFin. Field Inventory (FI), Forest Structural Complexity Tool (FSCT), 3D Forest Inventory (3DFin), Total number of trees (n). Pinewoods include both *P. halepensis* and *P. pinea.* Cypress includes *Cupressus sempervirens* while oak is *Quercus faginea*.

	FI	FSCT		3DFin	
	n	**Detected Trees**	**Detection Rate (%)**	**Detected Trees**	**Detection Rate (%)**
Pinewoods	93	89	95.6%	90	96.7%
Cypress	30	27	90.0%	25	83.3%
Oak	34	8	23.5%	18	52.9%
Total	157	124	79.0%	133	84.7%

When evaluating tree size attributes, results were remarkably different. FSCT substantially outperformed 3DFin in *h* estimation, with notably higher R^2 and lower RMSE across all metrics (Table 4). For *dbh*, both tools performed comparably.

Based on this comparison, HLS data processed within the FSCT algorithm were selected for subsequent SNFI-based tree volume calculation. The comparison between FI measurements and FSCT estimations of tree *dbh* and *h* are shown in Figure 8a,b.

Table 4. Statistical comparison of tree size attributes derived from HLS LiDAR data using FSCT and 3DFin algorithms against field inventory (FI) measurements.

Comparison with FI	*h* (m)		*dbh* (cm)	
	FSCT	3DFin	FSCT	3DFin
R^2	**0.87**	0.67	**0.86**	0.84
RMSE	**0.98**	1.61	**3.21**	3.64
MAPE (%)	**7.14**	12.19	**8.18**	11.11

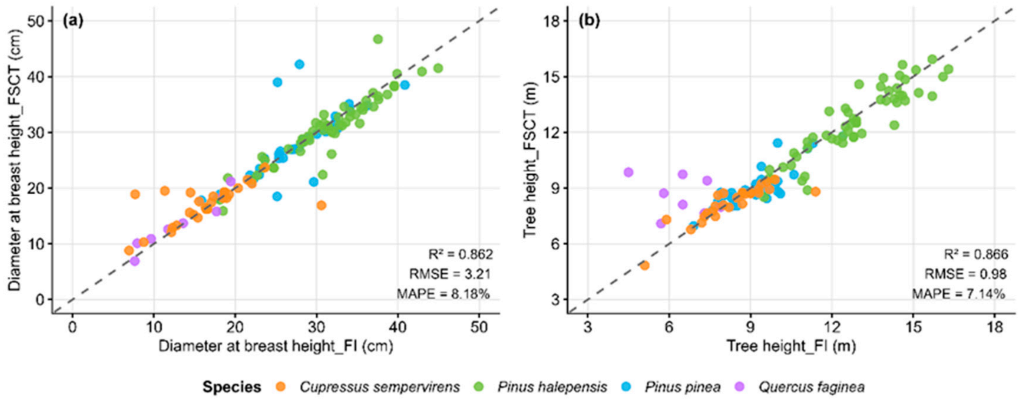

Figure 8. Comparison of FI and FSCT attributes (**a**) *dbh* comparison (**b**) *h* comparison. Each tree species is represented in different colors. R-square (R^2), Root Mean Square Error (RMSE), Mean Absolute Percentage Error (MAPE).

Stem volumes derived from FSCT-extracted *dbh* and *h* showed strong agreement with those calculated from field-based measurements using the same SNFI allometric equations (R^2 = 0.907, RMSE = 58.9 dm^3, MAPE = 18.06%), confirming that FSCT-derived tree attributes can reliably reproduce field-based SNFI volume estimates (Figure 9). This result supports their use as the dependent variable in subsequent RF model development.

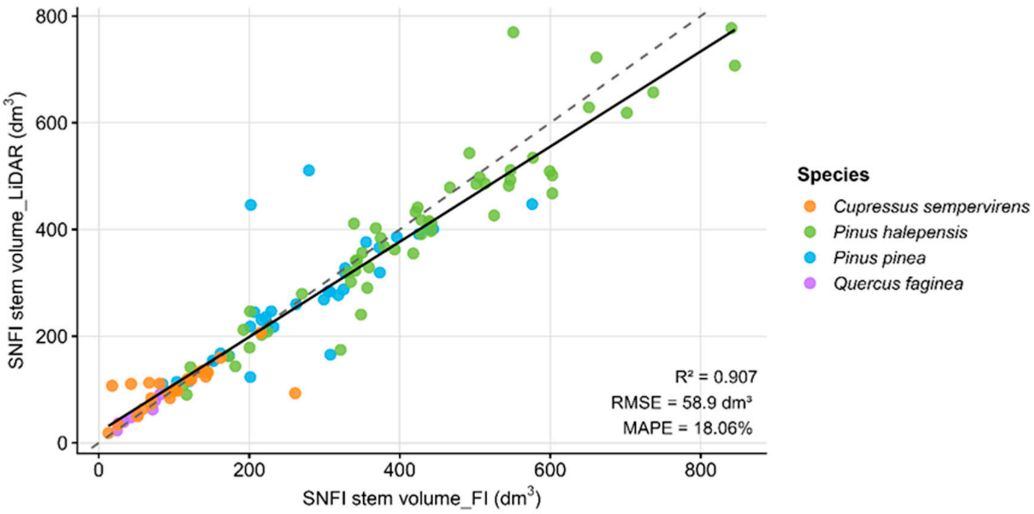

Figure 9. Comparison of stem volume calculated from field-measured tree attributes (x-axis) versus HLS-FSCT-derived tree attributes (y-axis), both using the SNFI allometric equations. Each point represents an individual tree, colored by species. The dashed line represents the 1:1 line of perfect agreement between methods; the solid line represents the fitted linear regression between the two volume estimates. R-square (R^2), Root Mean Square Error (RMSE), and Mean Absolute Percentage Error (MAPE) quantify the agreement between field-based and LiDAR-based volume estimates.

The 80 × 80 F configuration produced a point cloud density of approximately 580 points/m^2, while 80 × 60 CF yielded approximately 290 points/m^2 (both values refer to the raw reconstructed point clouds prior to height normalization and filtering). After extracting crown metrics using *lidRmetrics* R package [51], there were more than 70 structural and geometric features per tree, including crown area, height percentiles, crown volume proxies, convexity indices, and canopy shape descriptors. Among them, the estimated tree heights (zq95; the 95th height percentile of points within the crown, used as a proxy for tree top height) were compared with field measurements, where the 80 × 80 F point cloud showed strong agreement with field measurements (R^2 = 0.87, RMSE = 0.94 m), with the 80 × 60 CF configuration performing slightly lower (R^2 = 0.81, RMSE = 1.13 m).

3.2. Stem Volume Modeling

RF models developed separately for each flight configuration used SNFI-based stem volumes from FSCT-derived tree attributes as the dependent variable and selected UAV-SfM crown metrics (Table 5) as predictors.

Table 5. Selected crown metrics used as independent variables for two models. 80% front and side overlapping flight (80 × 80 F), 80% front and 60% side overlapping cross flight (80 × 60 CF). The selected variables are non-transformed.

	80 × 80 F Model		**80 × 60 CF Model**	
1	zq80	(80th height percentile)	zq90	(90th height percentile)
2	L2	(L-moment 2)	L2	(L-moment 2)
3	pzabove5	(proportion of points above 5 m)	vzrumple	(vertical rugosity)
4	CRR	(canopy relief ratio)	vFRcanopy	(canopy fill ratio)
5	zpcum9	(cumulative proportion at stratum 9)	pz_2.5	(proportion of points below 2.5 m)
6	vFRall	(full-fill ratio)		
7	Lskew	(L-skewness)		

The 80 × 80 F model, built on seven selected crown metrics, achieved R^2 = 0.730 and RMSE = 91.16 dm^3 on the held-out test dataset (seed = 123). The 80 × 60 CF model, built on five selected crown metrics, achieved R^2 = 0.688 and RMSE = 93.39 dm^3. To provide a spatially independent assessment of model generalizability, LOPO-CV was additionally performed. In this, each of the nine plots was sequentially withheld as the test set while the model was trained on the remaining plots. LOPO-CV yielded R^2 = 0.627 (RMSE = 108.25 dm^3) for the 80 × 80 F model and R^2 = 0.613 (RMSE = 111.95 dm^3) for the 80 × 60 CF model, representing more conservative estimates of predictive accuracy under spatial independence, as expected given that trees within the same plot share similar structural conditions. The marginal difference in model performance between the two flight configurations is broadly consistent with the twofold difference in point cloud density (580 points/m^2 and 290 points/m^2, respectively), suggesting that higher image overlap contributes to more informative crown metric extraction.

4. Discussion

4.1. HLS LiDAR Performance

Data processed from HLS LiDAR yielded varying results depending on the evaluated species. Higher detection accuracy was observed for pinewood and cypress, which constitute the mature canopy layer, far higher than oak (FSCT: 23.5%; 3DFin: 52.9%). Part of this gap reflects errors well documented in FSCT processing of structurally complex forests [41]: *Pinus halepensis* stems forking above breast height were occasionally recorded as separate individuals (Figure S1 in Supplementary Material), and branches were some-times misidentified as independent stems. This reflects limitations of current segmentation approaches rather than deficiencies specific to either tool. The larger driver, however, is oak's growth form: originating from natural regeneration favoured by thinning interventions, oak forms dense clusters in a secondary understory layer with small dimensions (mean *dbh* = 10.77 cm). This clustering mimics the effect of low branches on LiDAR stem recognition, compounded by tree size, since automated recognition is already known to struggle below 10 cm *dbh* [7,56,57]. These detection errors propagate into stand-level estimates such as density [58] and mean diameter [59].

Set against published terrestrial-LiDAR benchmarks, the detection rates obtained here are lower than those typically reported for structurally simple, single-species stands, where automated tools consistently reach around 90% [41,60–62], but fall within the range reported for mixed or multi-layered stands more comparable to ours [7,25,57,63]. This supports stand structure; overlapping crowns, irregular stem form, and multi-stemmed understory species, as the dominant constraint on detection, rather than tool performance [22,57,59,64], and points to dedicated algorithm development for multi-stemmed understory species as a clear priority for future work.

The *h* estimates showed a related but more nuanced pattern. Across the stand, ground-based scanners tended to underestimate height, a well-known consequence of sparse point density in the upper canopy [7,22,41] that manifested here as incomplete treetop capture by ground-based LiDAR scanners (Figure S2 in Supplementary Material). Merging ground-based point clouds with ALS data has been proposed to address this [56,65], though at the cost of the simplicity that makes the present open-source workflow attractive. For oak specifically, the pattern reversed: FSCT consistently overestimated *h*, most likely because canopy points from neighboring crowns and overstorey pines were misassigned to oak individuals, which have the same clustered, multi-stemmed structure that is responsible for the detection errors above. Some studies have adopted clump-level measurement for resprouting hardwood species: using clump height and whole-clump LiDAR volume rather than individual stem attributes, and reported good results for biomass estimation [66], suggesting this approach could benefit structurally similar understory species like *Q. faginea*. It is also worth noting that the field reference itself is not error-free: hypsometer height measurements carry observer-dependent uncertainty, so part of the apparent error attributed to HLS may instead reflect bias in the reference values [67–69].

dbh estimation was comparably accurate for both tools, consistent with the established strength of ground-based LiDAR for stem-level measurement, where dense near-ground point clouds support reliable circular cross-section fitting [7,22,41]. The somewhat higher *dbh* error observed here relative to comparable Mediterranean stands [56] is attributable to the inclusion of smaller trees (*dbh* $\geq$ 7 cm); as with detection, point cloud-based *dbh* estimation is known to lose accuracy below 10 cm [7,59,70]. Taken together, these component-level errors did not undermine the practical value of the workflow: cross-method validation showed that FSCT-derived *dbh* and *h* reproduced field-based SNFI volumes with high fidelity (R^2 = 0.907), confirming that FSCT's attribute estimates are reliable enough to support operational stem volume estimation despite known limitations around forking stems and branch misidentification.

It is important to acknowledge that this cross-method validation assessed the consistency between two applications of the same SNFI allometric equation, one to field-measured *dbh* and *h*, the other to FSCT-derived *dbh* and *h*, rather than independently validating the allometric equation itself. Consequently, the high agreement (R^2 = 0.907) primarily reflects the accuracy of FSCT in replicating field-measured tree attributes, and should not be interpreted as a validation of the absolute volume estimates produced by the SNFI equations. Two distinct sources of uncertainty affect the final reference volumes used as RF model targets: first, errors in FSCT-derived *dbh* and *h* (RMSE = 3.21 cm and 0.98 m respectively), which propagate through the allometric equation of the SNFI model ($vcc = p \cdot dbh^q \cdot h^r$); and second, the uncertainty of the allometric equations themselves, which were parameterized on historical datasets and may not fully represent contemporary growth conditions in the study stand [15,16]. Together, these limitations suggest that the absolute volume values predicted by the RF models carry compound uncertainty beyond what the R^2 metrics alone convey, and should be treated as operationally useful approximations rather than precise individual-tree volume measurements.

4.2. Modeling Individual Stem Volume Based on UAV-SfM Performance

Beyond ground-based attribute extraction, the second phase of this study tested whether canopy structure captured by UAV-SfM could support individual-tree volume prediction directly, complementing the HLS-derived attributes above. Flight configuration was the central methodological decision here, given its direct bearing on output quality; prior comparisons of flight configurations span contexts as different as urban mapping [71] and forestry applications [35,45,72], the latter of which more closely mirrors the present case. Two configurations were compared: an 80 × 80 F nadir flight, following the RGB protocol of [34], and an 80 × 60 CF cross-flight intended to improve visibility of understory trees by capturing them from multiple angles, as reported beneficial elsewhere [73]. Contrary to this expectation, the two configurations produced comparable model accuracy, with 80 × 80 F performing marginally better despite its simpler design-consistent with other studies finding nadir flights outperform oblique or cross configurations [35,74]. Ref. [35] notes that while oblique imagery can still add understory information, current analysis algorithms have yet to fully exploit it, which may explain why the added complexity of 80 × 60 CF produced no measurable gain here. As with the HLS analysis above, automated individual-tree detection from UAV-SfM proved difficult in this mixed canopy of planted conifers and oak regeneration, echoing prior work on tree-top identification in mixed conifer stands [75] and on the limited improvement of increasing image overlap beyond 80% side-overlap [35]. Consequently, manual delineation was adopted to avoid introducing detection bias into the volume models.

The low oak detection rate (23.5% by FSCT) has direct implications for volume prediction that extend beyond tree detection alone. Oak individuals successfully detected and matched represent a non-random subsample—likely biased toward larger, more structurally distinct stems that are more easily resolved from dense understory clusters—meaning the RF models cannot be considered representative of oak volume variability across its full-size range in the stand. Given this severely limited and potentially biased oak representation in both training and test datasets, species-level accuracy assessment for oak is not statistically meaningful, and the RF models developed here should be considered validated only for the dominant conifer species groups. In stands where broadleaf understory species represent a significant proportion of stand volume—as is increasingly the case following natural regeneration and thinning interventions in Mediterranean forests—this detection limitation represents a meaningful constraint on operational applicability. Addressing the detection limitations documented for oaks will require dedicated methodological development. Two complementary directions appear promising: first, adopting clump-level measurement approaches—treating multi-stemmed individuals as single structural units for height and volume estimation rather than attempting discrete stem delineation—has shown good results for biomass estimation in resprouting tree species [66] and warrants exploration for *Q. faginea* in future forest inventory workflows. Second, deep learning frameworks for 3D point cloud segmentation have demonstrated substantially improved accuracy for automated individual tree delineation across diverse forest types compared to conventional rule-based methods [8], and represent a promising avenue for resolving the clustered, multi-stemmed growth forms that current automated tools consistently struggle with in structurally complex mixed stands.

Despite the detection challenge, UAV-derived point clouds yielded reliable height estimates under both configurations, with 80 × 80 F again performing marginally better-consistent with its higher point density and the well-established relationship between image overlap and 3D canopy reconstruction quality [27,72,76]. These crown metrics in turn supported reasonable volume predictions (R^2 = 0.730 and 0.688 for 80 × 80 F and 80 × 60 CF, respectively), driven primarily by height percentiles, canopy fill ratios, and vertical distribution descriptors, reflecting the established link between crown architecture and stem volume, where taller, more densely filled crowns correspond to larger stems [29,76]. That both above- and below-stratum metrics (pzabove5, pz_2.5) contributed to the final models indicates that the full vertical profile of an individual tree's own crown, not maximum height alone, carries predictive information for its stem volume; consistent with evidence that within-crown vertical structure explains meaningful additional variance in individual-tree volume and biomass models beyond height alone [29,77].

These R^2 values sit within the 0.70–0.80 range commonly reported for RF-based volume models from UAV-SfM data in structurally complex mixed forests with limited plot samples [31,77], consistent with RF's established robustness as a predictive modeling algorithm across diverse remote sensing applications [78]. That comparable accuracy was achieved here with only nine plots suggests the workflow is performing near the ceiling of what this sample size can support; increasing plot replication therefore remains the most direct route to improving model robustness [77,79–81].

Model accuracy estimates varied according to the validation approach applied, as expected given the limited sample size. Test-set R^2 values (0.730 and 0.688 for 80 × 80 F and 80 × 60 CF, respectively) represent an upper bound of predictive accuracy under the specific random partition used. LOPO-CV R^2 (0.627 and 0.613) provides a more conservative and spatially independent estimate, accounting for the fact that trees within the same plot share similar structural conditions and cannot be considered independent observations. The consistency between test-set and LOPO-CV results across both configurations, with 80 × 80 F outperforming 80 × 60 CF under both validation approaches, confirms that the performance difference between flight configurations is genuine rather than an artefact of the specific partition used.

A related limitation, and one not addressed in this study despite the species-driven performance differences documented above, is species identification. In open, single-layered Mediterranean pinewoods, combining low-density LiDAR with satellite imagery has produced good species-classification results [82], but this task becomes substantially harder as structural complexity increases, for at least three reasons. First, scanner type itself affects identification accuracy: comparisons across multispectral, monospectral, and single-photon airborne systems show that classification performance is not interchangeable across sensor types [83]. Second, both the identification technique and the specific species composition involved matter, since classification accuracy in complex coniferous–broadleaf mixed forests has been shown to vary considerably between species rather than applying uniformly across a stand [84]. Critically, this means species identification models cannot simply be transferred from one forest condition to another, i.e., performance calibrated in open pinewoods, or even in a different mixed stand, cannot be assumed to hold in the two-layered conifer–oak structure studied here, underscoring the need for region- or stand-specific model development rather than a single generalizable solution.

Our finding is consistent with another study, which reported that UAV-based sensing alone, whether LiDAR or photogrammetry, is insufficient for individual-tree stem volume prediction when only crown information is available, and similarly concluded that integration with ground-based LiDAR is necessary for reliable volume estimation [36]. It is important to highlight that most of our workflow was supported by affordable, open-source tools, with the sole exception of the HLS LiDAR data processing. While this device relies on proprietary software, it was used exclusively to convert the raw output files (.geoslam) into a standard, non-proprietary format (.las) for subsequent analysis within open-source tools. Furthermore, this step could be omitted from the workflow and replaced by traditional forest inventory methods, thereby eliminating acquisition costs. This flexibility demonstrates that forest managers, landowners, and researchers can successfully access and reproduce the model and estimate stem volume across large forested areas using low-cost, consumer-grade RGB drones.

Collectively, the limitations identified across the processing pipeline-from ground-based detection constraints to UAV-SfM crown metric extraction and model transferability-point toward a clear development agenda for this type of integrated workflow. Expanding the sampling framework to include additional plots and stand types remains the most immediate priority, as model robustness is currently bounded by the available training data. Over the longer term, advances in automated segmentation algorithms and deep learning-based point cloud analysis are likely to reduce the manual intervention currently required for tree matching and detection of structurally complex understory species, broadening the operational applicability of predominantly open-source workflows like the one demonstrated here.

5. Conclusions

This study demonstrates that integrating HLS with UAV-based SfM photogrammetry through a predominantly open-source workflow is a viable, reproducible approach for automated individual-tree stem volume modeling in Mediterranean mixed forest stands. Four main conclusions emerge from the results.

First, FSCT outperformed 3DFin in tree attribute estimation, particularly for *h*, and was selected for SNFI-based stem volume calculation. Second, cross-method validation confirmed strong agreement between FSCT-derived and field-measured SNFI volumes (R^2 = 0.907), supporting the use of HLS-derived attributes as a reliable substitute for labor-intensive individual tree measurement in standard Spanish forest inventory practice. Third, the 80 × 80 F UAV flight configuration outperformed 80 × 60 CF in both point cloud density and *h* estimation accuracy, yielding a marginally superior volume model (R^2 = 0.730 vs. 0.688), demonstrating that a single high-overlap nadir flight is sufficient for crown-based volume modeling without the added complexity of cross-flight patterns. Fourth, RF models trained on UAV-SfM crown metrics achieved moderate-to-high predictive accuracy for both configurations (test R^2 = 0.730 and 0.688; LOPO-CV R^2 = 0.627 and 0.613), confirming that photogrammetric crown structure captures sufficient information to predict individual-tree stem volume when calibrated against HLS-derived reference volumes, while the spatially independent LOPO-CV estimates confirm the robustness of these results beyond the specific training partition used.

Together, these findings support HLS and UAV-SfM integration as a cost-effective, predominantly open-source framework for complementing traditional forest inventory in structurally complex Mediterranean mixed stands. The use of consumer-grade RGB UAV sensors and predominantly open-source processing tools lowers the entry barrier for forest managers and researchers operating under budget constraints. Key practical limitations should nonetheless be considered before operational deployment: the workflow depends on SNFI allometric equations as reference volume standards, limiting direct transferability where such equations are unavailable or poorly parameterised, and model performance is sensitive to training sample size. Future work should therefore prioritize expanding plot replication, improving detection algorithms for multi-stemmed understory species, and testing the workflow across a broader range of forest types and regions.

Supplementary Materials: The following supporting information can be downloaded at: https://www.mdpi.com/article/10.3390/f17080944/s1, Figure S1: Field photograph of a *Pinus halepensis* individual exhibiting stem forking above breast height. Cases such as this were occasionally misclassified by FSCT as two separate tree individuals during point cloud segmentation, contributing to localized over detection errors; Figure S2: Side-view profile of an HLS point cloud colored by height above the digital terrain model (DTM), illustrating sparse point density in the upper canopy (yellow-red, >12 m). This reduced point density at treetop level is consistent with incomplete treetop capture by ground-based laser scanning, contributing to height underestimation relative to field measurements.

Author Contributions: C.T.M.D.: Writing—original draft, conceptualization, methodology, data curation, investigation, formal analysis, validation, visualization. F.T.-S.: Writing—review & editing, supervision, conceptualization, methodology, data curation, formal analysis, validation. A.V.-V.: Writing—review & editing, supervision, conceptualization, methodology, data curation, formal analysis, validation. F.B.: Writing—review & editing, supervision, conceptualization, methodology, validation, project administration, funding acquisition. All authors have read and agreed to the published version of the manuscript.

Funding: This research was funded by, 1. MEDFOR Master Programme on Mediterranean Forestry and Natural Resources Management (Erasmus+: Erasmus Mundus Joint Master Degrees, Project Reference 619801-EPP-1-2020-1-PT-EPPKA1-JMD-MOB). 2. Predoctoral contract (Call 2024) at the University of Valladolid, Spain (BOCyL of May 18). 3. IMFLEX Grant PID2021-126275OB-C22-Integrated Forest Management along complexity gradients, funded by the Spanish Government (Ministerio de Ciencia e Innovación MCIN/AEI/10.13039/501100011033). Additional funding for this study was provided by, 1. ETN Skill-For-Action project from the European Union's Horizon 2020 research and innovation program under the Marie Skłodowska-Curie, Grant Agreement #956355. 2. Project 'CLU-2025-2-07′ iuFOR Institute Unit of Excellence' and its International Reinforce (CL-EI-2021-05) at the University of Valladolid funded by the Junta de Castilla and co-financed by the European Union (ERDF "Europe drives our growth"). 3. European Union and Junta de Castilla y León Education Council (ORDEN EDU/842/2022).

Data Availability Statement: The LiDAR point clouds, UAV imagery, and derived datasets of the current study are not publicly available due to ongoing research activities but are available from the corresponding author upon reasonable request.

Acknowledgments: We are grateful to Cristóbal Ordóñez for his support in data collection and project administration, and to Andrés Bravo Núñez for assistance with statistical analysis. We also thank the open-source software community for providing reliable tools, and the Regional Forest Service at Palencia for implementing the thinning treatments and granting permission to conduct our study.

Conflicts of Interest: The authors declare that they have no known competing financial interests or personal relationships that could have appeared to influence the work reported in this paper.

References

1. Gauquelin, T. *Specificity and Universality of Forestal Mediterranean Ecosystems*; Nova Science Publishers, Inc.: New York, NY, USA, 2011.
2. Gauquelin, T.; Michon, G.; Joffre, R.; Duponnois, R.; Génin, D.; Fady, B.; Bou Dagher-Kharrat, M.; Derridj, A.; Slimani, S.; Badri, W.; et al. Mediterranean Forests, Land Use and Climate Change: A Social-Ecological Perspective. *Reg. Environ. Change* **2018**, *18*, 623–636. [CrossRef]

3. Martín-López, B.; Oteros-Rozas, E.; Cohen-Shacham, E.; Santos-Martín, F.; Nieto-Romero, M.; Carvalho-Santos, C.; González, J.A.; García-Llorente, M.; Klass, K.; Geijzendorffer, I.; et al. Ecosystem Services Supplied by Mediterranean Basin Ecosystems. In *Routledge Handbook of Ecosystem Services*; Potschin, M., Haines-Young, R., Fish, R., Turner, R.K., Eds.; Routledge: New York, NY, USA, 2016; pp. 405–414.
4. Bravo, F.; Martín Ariza, A.; Dugarsuren, N.; Ordóñez, C. Disentangling the Relationship between Tree Biomass Yield and Tree Diversity in Mediterranean Mixed Forests. *Forests* **2021**, *12*, 848. [CrossRef]
5. Nocentini, S.; Travaglini, D.; Muys, B. Managing Mediterranean Forests for Multiple Ecosystem Services: Research Progress and Knowledge Gaps. *Curr. For. Rep.* **2022**, *8*, 229–256. [CrossRef]
6. Álvarez-González, J.G.; Cañellas, I.; Alberdi, I.; Gadow, K.V.; Ruiz-González, A.D. National Forest Inventory and Forest Observational Studies in Spain: Applications to Forest Modeling. *For. Ecol. Manag.* **2014**, *316*, 54–64. [CrossRef]
7. Bauwens, S.; Bartholomeus, H.; Calders, K.; Lejeune, P. Forest Inventory with Terrestrial LiDAR: A Comparison of Static and Hand-Held Mobile Laser Scanning. *Forests* **2016**, *7*, 127. [CrossRef]
8. Xiang, B.; Wielgosz, M.; Kontogianni, T.; Peters, T.; Puliti, S.; Astrup, R.; Schindler, K. Automated Forest Inventory: Analysis of High-Density Airborne LiDAR Point Clouds with 3D Deep Learning. *Remote Sens. Environ.* **2024**, *305*, 114078. [CrossRef]
9. Husch, B.; Beers, T.W.; Kershaw, J.A. *Forest Mensuration*, 4th ed.; J. Wiley: New York, NY, USA, 2003.
10. Ruiz-Peinado, R.; Del Rio, M.; Montero, G. New Models for Estimating the Carbon Sink Capacity of Spanish Softwood Species. *For. Syst.* **2011**, *20*, 176–188. [CrossRef]
11. Bravo, F.; Alvarez-Gonzalez, J.G.; Del Rio, M.; Barrio, M.; Bonet, J.A.; Bravo-Oviedo, A.; Calama, R.; Castedo-Dorado, F.; Crecente-Campo, F.; Condes, S.; et al. Growth and Yield Models in Spain: Historical Overview, Contemporary Examples and Perspectives. *For. Syst.* **2011**, *20*, 315–328. [CrossRef]
12. Ruiz-Peinado Gertrudix, R.; Montero, G.; Del Rio, M. Biomass Models to Estimate Carbon Stocks for Hardwood Tree Species. *For. Syst.* **2012**, *21*, 42–52. [CrossRef]
13. Vatandaşlar, C.; Zeybek, M. Application of Handheld Laser Scanning Technology for Forest Inventory Purposes in the NE Turkey. *Turk. J. Agric. For.* **2020**, *44*, 229–242. [CrossRef]
14. Kershaw, J.A.; Ducey, M.J.; Beers, T.W.; Husch, B. *Forest Mensuration*, 1st ed.; Wiley: New York, NY, USA, 2016.
15. Alberdi, I.; Cañellas, I.; Vallejo Bombín, R. The Spanish National Forest Inventory: History, Development, Challenges and Perspectives. *Pesqui. Florest. Bras.* **2017**, *37*, 361–368. [CrossRef]
16. Cantero Amiano, A. Variación de La Relación Altura-Diámetro a Lo Largo Del Tiempo En Un Macizo Forestal. In Proceedings of the 6CFE01-480, Sociedad Española de Ciencias Forestales, Vitoria-Gasteiz, Spain, 10–14 June 2013.
17. Crecente-Campo, F.; Rojo Alboreca, A.; Diéguez-Aranda, U. A Merchantable Volume System for Pinus Sylvestris L. in the Major Mountain Ranges of Spain. *Ann. For. Sci.* **2009**, *66*, 808. [CrossRef]
18. Gómez-García, E.; Crecente-Campo, F.; Diéguez-Aranda, U. Selection of Mixed-Effects Parameters in a Variable–Exponent Taper Equation for Birch Trees in Northwestern Spain. *Ann. For. Sci.* **2013**, *70*, 707–715. [CrossRef]
19. Arias-Rodil, M.; Diéguez-Aranda, U.; Rodríguez Puerta, F.; López-Sánchez, C.A.; Canga Líbano, E.; Cámara Obregón, A.; Castedo-Dorado, F. Modelling and Localizing a Stem Taper Function for *Pinus Radiata* in Spain. *Can. J. For. Res.* **2015**, *45*, 647–658. [CrossRef]
20. Brede, B.; Calders, K.; Lau, A.; Raumonen, P.; Bartholomeus, H.M.; Herold, M.; Kooistra, L. Non-Destructive Tree Volume Estimation through Quantitative Structure Modelling: Comparing UAV Laser Scanning with Terrestrial LIDAR. *Remote Sens. Environ.* **2019**, *233*, 111355. [CrossRef]
21. Lee, Y.; Lee, J. Advancing Stem Volume Estimation Using Multi-Platform LiDAR and Taper Model Integration for Precision Forestry. *Remote Sens.* **2025**, *17*, 785. [CrossRef]
22. Liang, X.; Kankare, V.; Hyyppä, J.; Wang, Y.; Kukko, A.; Haggrén, H.; Yu, X.; Kaartinen, H.; Jaakkola, A.; Guan, F.; et al. Terrestrial Laser Scanning in Forest Inventories. *ISPRS J. Photogramm. Remote Sens.* **2016**, *115*, 63–77. [CrossRef]
23. Gollob, C.; Ritter, T.; Nothdurft, A. Forest Inventory with Long Range and High-Speed Personal Laser Scanning (PLS) and Simultaneous Localization and Mapping (SLAM) Technology. *Remote Sens.* **2020**, *12*, 1509. [CrossRef]
24. Solares-Canal, A.; Alonso, L.; Picos, J.; Armesto, J. Automatic Tree Detection and Attribute Characterization Using Portable Terrestrial Lidar. *Trees* **2023**, *37*, 963–979. [CrossRef]
25. Tupinambá-Simões, F.; Pascual, A.; Guerra-Hernández, J.; Ordóñez, C.; De Conto, T.; Bravo, F. Assessing the Performance of a Handheld Laser Scanning System for Individual Tree Mapping—A Mixed Forests Showcase in Spain. *Remote Sens.* **2023**, *15*, 1169. [CrossRef]
26. Kükenbrink, D.; Marty, M.; Rehush, N.; Abegg, M.; Ginzler, C. Evaluating the Potential of Handheld Mobile Laser Scanning for an Operational Inclusion in a National Forest Inventory—A Swiss Case Study. *Remote Sens. Environ.* **2025**, *321*, 114685. [CrossRef]
27. Goodbody, T.R.H.; Coops, N.C.; White, J.C. Digital Aerial Photogrammetry for Updating Area-Based Forest Inventories: A Review of Opportunities, Challenges, and Future Directions. *Curr. For. Rep.* **2019**, *5*, 55–75. [CrossRef]

28. Iglhaut, J.; Cabo, C.; Puliti, S.; Piermattei, L.; O'Connor, J.; Rosette, J. Structure from Motion Photogrammetry in Forestry: A Review. *Curr. For. Rep.* **2019**, *5*, 155–168. [CrossRef]
29. Liao, K.; Li, Y.; Zou, B.; Li, D.; Lu, D. Examining the Role of UAV Lidar Data in Improving Tree Volume Calculation Accuracy. *Remote Sens.* **2022**, *14*, 4410. [CrossRef]
30. Neuville, R.; Bates, J.S.; Jonard, F. Estimating Forest Structure from UAV-Mounted LiDAR Point Cloud Using Machine Learning. *Remote Sens.* **2021**, *13*, 352. [CrossRef]
31. Puliti, S.; Ene, L.T.; Gobakken, T.; Næsset, E. Use of Partial-Coverage UAV Data in Sampling for Large Scale Forest Inventories. *Remote Sens. Environ.* **2017**, *194*, 115–126. [CrossRef]
32. Munteanu, D.; Moldovanu, S.; Murariu, G.; Dinca, L. Sustainable Estimation of Tree Biomass and Volume Using UAV Imagery: A Comprehensive Review. *Sustainability* **2026**, *18*, 1095. [CrossRef]
33. Swayze, N.C.; Tinkham, W.T.; Vogeler, J.C.; Hudak, A.T. Influence of Flight Parameters on UAS-Based Monitoring of Tree Height, Diameter, and Density. *Remote Sens. Environ.* **2021**, *263*, 112540. [CrossRef]
34. Maes, W.H. Practical Guidelines for Performing UAV Mapping Flights with Snapshot Sensors. *Remote Sens.* **2025**, *17*, 606. [CrossRef]
35. Young, D.J.N.; Koontz, M.J.; Weeks, J. Optimizing Aerial Imagery Collection and Processing Parameters for Drone-based Individual Tree Mapping in Structurally Complex Conifer Forests. *Methods Ecol. Evol.* **2022**, *13*, 1447–1463. [CrossRef]
36. Hoshikawa, T.; Suzuki, S.; Yajima, J.; Mochizuki, H.; Yamamoto, K. Integrating Personal Laser Scanning with Uncrewed Aerial Vehicle-Based Photogrammetry or Laser Scanning for Accurate Stem Volume Estimation in Temperate Coniferous Forests. *J. For. Res.* **2024**, *29*, 343–351. [CrossRef]
37. Climate-Data.org. Available online: https://es.climate-data.org/europe/espana/castilla-y-leon/palencia-2155/ (accessed on 13 June 2024).
38. *FARO Connect Software*, Version 2025.0.0; FARO: Lake Mary, FL, USA, 2025.
39. *Topcon Magnet Office Software*, Version 9.0; Topcon Positioning Group: Livermore, CA, USA, 2024.
40. R Core Team. *R: A Language and Environment for Statistical Computing, Version 4.4.1*; R Foundation for Statistical Computing: Vienna, Austria, 2025.
41. Krisanski, S.; Taskhiri, M.S.; Gonzalez Aracil, S.; Herries, D.; Muneri, A.; Gurung, M.B.; Montgomery, J.; Turner, P. Forest Structural Complexity Tool—An Open Source, Fully-Automated Tool for Measuring Forest Point Clouds. *Remote Sens.* **2021**, *13*, 4677. [CrossRef]
42. Laino, D.; Cabo, C.; Prendes, C.; Janvier, R.; Ordonez, C.; Nikonovas, T.; Doerr, S.; Santin, C. 3DFin: A Software for Automated 3D Forest Inventories from Terrestrial Point Clouds. *For. Int. J. For. Res.* **2024**, *97*, 479–496. [CrossRef]
43. *Cloud Compare, 3D Point Cloud and Mesh Processing Software*, Version 2.13.2 2024; EDF R&D: Paris, France, 2024.
44. Ministerio para la Transición Ecológica y el Reto Demográfico. *IFN4 Cuarto Inventario Forestal Nacional (IFN4)*; Ministerio para la Transición Ecológica y el Reto Demográfico: Madrid, Spain, 2022.
45. Dandois, J.; Olano, M.; Ellis, E. Optimal Altitude, Overlap, and Weather Conditions for Computer Vision UAV Estimates of Forest Structure. *Remote Sens.* **2015**, *7*, 13895–13920. [CrossRef]
46. *WebODM, OpenDroneMap Software*, Version v2.4.2 2024; Piero Toffanin: St. Petersburg, FL, USA, 2024.
47. Roussel, J.-R.; Auty, D. *lidR: Airborne LiDAR Data Manipulation and Visualization for Forestry Applications 2023*, R package version 3.1.0; R Archive Network: Vienna, Austria, 2016.
48. Roussel, J.-R.; Auty, D.; Coops, N.C.; Tompalski, P.; Goodbody, T.R.H.; Meador, A.S.; Bourdon, J.-F.; De Boissieu, F.; Achim, A. lidR: An R Package for Analysis of Airborne Laser Scanning (ALS) Data. *Remote Sens. Environ.* **2020**, *251*, 112061. [CrossRef]
49. Zhang, K.; Chen, S.C.; Whitman, D.; Shyu, M.L.; Yan, J.; Zhang, C. A Progressive Morphological Filter for Removing Nonground Measurements from Airborne LIDAR Data. *IEEE Trans. Geosci. Remote Sens.* **2003**, *41*, 872–882. [CrossRef]
50. Silva, C.A.; Hudak, A.T.; Vierling, L.A.; Loudermilk, E.L.; O'Brien, J.J.; Hiers, J.K.; Jack, S.B.; Gonzalez-Benecke, C.; Lee, H.; Falkowski, M.J.; et al. Imputation of Individual Longleaf Pine (*Pinus Palustris* Mill.) Tree Attributes from Field and LiDAR Data. *Can. J. Remote Sens.* **2016**, *42*, 554–573. [CrossRef]
51. Tompalski, P. *lidRmetrics: Point Cloud Metrics for the lidR Package*; R Package Version 0.1.5; R Archive Network: Vienna, Austria, 2025.
52. QGIS Development Team. QGIS Geographic Information System, Version 3.44, Open Source Geospatial Foundation. 2025. Available online: https://qgis.org/ (accessed on 20 August 2025).
53. Breiman, L. Random Forests. *Mach. Learn.* **2001**, *45*, 5–32. [CrossRef]
54. Liaw, A.; Wiener, M. Classification and Regression by randomForest. *R News* **2002**, *2*, 18–22.
55. Kuhn, M. Building Predictive Models in *R* Using the Caret Package. *J. Stat. Softw.* **2008**, *28*, 1–26. [CrossRef]
56. Giannetti, F.; Puletti, N.; Quatrini, V.; Travaglini, D.; Bottalico, F.; Corona, P.; Chirici, G. Integrating Terrestrial and Airborne Laser Scanning for the Assessment of Single-Tree Attributes in Mediterranean Forest Stands. *Eur. J. Remote Sens.* **2018**, *51*, 795–807. [CrossRef]

57. Comesaña-Cebral, L.; Martínez-Sánchez, J.; Lorenzo, H.; Arias, P. Individual Tree Segmentation Method Based on Mobile Backpack LiDAR Point Clouds. *Sensors* **2021**, *21*, 6007. [CrossRef] [PubMed]
58. Vatandaşlar, C.; Seki, M.; Zeybek, M. Assessing the Potential of Mobile Laser Scanning for Stand-Level Forest Inventories in near-Natural Forests. *For. Int. J. For. Res.* **2023**, *96*, 448–464. [CrossRef]
59. Ryding, J.; Williams, E.; Smith, M.; Eichhorn, M. Assessing Handheld Mobile Laser Scanners for Forest Surveys. *Remote Sens.* **2015**, *7*, 1095–1111. [CrossRef]
60. Xia, S.; Wang, C.; Pan, F.; Xi, X.; Zeng, H.; Liu, H. Detecting Stems in Dense and Homogeneous Forest Using Single-Scan TLS. *Forests* **2015**, *6*, 3923–3945. [CrossRef]
61. González, R.A.; Gómez, C.C.; López, J.G.; Dorado, F.C.; Cuevas, C.Á.; Álvarez-Taboada, F. Is Handheld Mobile Scanner Data Operational for the Evaluation of Field Performance of Poplar Clones? In *Proceedings of the 2023 IEEE International Workshop on Metrology for Agriculture and Forestry (MetroAgriFor)*; IEEE: Pisa, Italy, 2023; pp. 618–623.
62. Arévalo-González, R.; Álvarez-Cuevas, C.; Cabo, C.; Castedodorad, F.; Álvarez-Taboada, F. Exactitud Del Escáner Láser Móvil Para Inventario y Cubicación de Choperas. Comparación Entre Escáneres (GeoSLAM ZEB Horizon y NavVis VLX 3) y Trayectorias de Medición. In *Proceedings of the Actas del Noveno Congreso Forestal Español*; Sociedad Española de Ciencias Forestales: Gijon, Spain, 2025.
63. Giannetti, F.; Passarino, L.; Aleandri, G.; Borghi, C.; Vangi, E.; Anzilotti, S.; Raddi, S.; Chirici, G.; Travaglini, D.; Maltoni, A.; et al. Efficiency of Mobile Laser Scanning for Digital Marteloscopes for Conifer Forests in the Mediterranean Region. *Forests* **2024**, *15*, 2202. [CrossRef]
64. Del Perugia, B.; Giannetti, F.; Chirici, G.; Travaglini, D. Influence of Scan Density on the Estimation of Single-Tree Attributes by Hand-Held Mobile Laser Scanning. *Forests* **2019**, *10*, 277. [CrossRef]
65. Paris, C.; Kelbe, D.; Van Aardt, J.; Bruzzone, L. A Precise Estimation of the 3D Structure of the Forest Based on the Fusion of Airborne and Terrestrial Lidar Data. In *Proceedings of the 2015 IEEE International Geoscience and Remote Sensing Symposium (IGARSS)*; IEEE: Milan, Italy, 2015; pp. 49–52.
66. Bell, D.; Halbur, M.; Elias, F.; Pearson, N.; Crocker, D.E.; Bentley, L.P. Assessing Umbellularia Californica Basal Resprouting Response Post-Wildfire Using Field Measurements and Ground-Based LiDAR Scanning. *Remote Sens.* **2025**, *17*, 3101. [CrossRef]
67. Wang, Y.; Lehtomäki, M.; Liang, X.; Pyörälä, J.; Kukko, A.; Jaakkola, A.; Liu, J.; Feng, Z.; Chen, R.; Hyyppä, J. Is Field-Measured Tree Height as Reliable as Believed—A Comparison Study of Tree Height Estimates from Field Measurement, Airborne Laser Scanning and Terrestrial Laser Scanning in a Boreal Forest. *ISPRS J. Photogramm. Remote Sens.* **2019**, *147*, 132–145. [CrossRef]
68. Ojoatre, S.; Zhang, C.; Hussin, Y.A.; Kloosterman, H.E.; Ismail, M.H. Assessing the Uncertainty of Tree Height and Aboveground Biomass From Terrestrial Laser Scanner and Hypsometer Using Airborne LiDAR Data in Tropical Rainforests. *IEEE J. Sel. Top. Appl. Earth Obs. Remote Sens.* **2019**, *12*, 4149–4159. [CrossRef]
69. Wertz, B.; Ochał, W.; Bronisz, K.; Orzeł, S. Effect of the Interaction between User Experience and Hypsometer Type on the Uncertainty of Ground-Based Tree Height Measurement. *For. Int. J. For. Res.* **2026**, *99*, cpaf022. [CrossRef]
70. Cabo, C.; Ordóñez, C.; López-Sánchez, C.A.; Armesto, J. Automatic Dendrometry: Tree Detection, Tree Height and Diameter Estimation Using Terrestrial Laser Scanning. *Int. J. Appl. Earth Obs. Geoinf.* **2018**, *69*, 164–174. [CrossRef]
71. Liu, Y.; Han, K.; Rasdorf, W. Assessment and Prediction of Impact of Flight Configuration Factors on UAS-Based Photogrammetric Survey Accuracy. *Remote Sens.* **2022**, *14*, 4119. [CrossRef]
72. Kuželka, K.; Surový, P. Mapping Forest Structure Using UAS inside Flight Capabilities. *Sensors* **2018**, *18*, 2245. [CrossRef] [PubMed]
73. Díaz, G.M.; Mohr-Bell, D.; Garrett, M.; Muñoz, L.; Lencinas, J.D. Customizing Unmanned Aircraft Systems to Reduce Forest Inventory Costs: Can Oblique Images Substantially Improve the 3D Reconstruction of the Canopy? *Int. J. Remote Sens.* **2020**, *41*, 3480–3510. [CrossRef]
74. Lamping, J.E.; Zald, H.S.J.; Madurapperuma, B.D.; Graham, J. Comparison of Low-Cost Commercial Unpiloted Digital Aerial Photogrammetry to Airborne Laser Scanning across Multiple Forest Types in California, USA. *Remote Sens.* **2021**, *13*, 4292. [CrossRef]
75. Mohan, M.; Silva, C.; Klauberg, C.; Jat, P.; Catts, G.; Cardil, A.; Hudak, A.; Dia, M. Individual Tree Detection from Unmanned Aerial Vehicle (UAV) Derived Canopy Height Model in an Open Canopy Mixed Conifer Forest. *Forests* **2017**, *8*, 340. [CrossRef]
76. Puliti, S.; Dash, J.P.; Watt, M.S.; Breidenbach, J.; Pearse, G.D. A Comparison of UAV Laser Scanning, Photogrammetry and Airborne Laser Scanning for Precision Inventory of Small-Forest Properties. *For. Int. J. For. Res.* **2020**, *93*, 150–162. [CrossRef]
77. Stereńczak, K.; Kraszewski, B.; Mielcarek, M.; Piasecka, Ż.; Lisiewicz, M.; Heurich, M. Mapping Individual Trees with Airborne Laser Scanning Data in an European Lowland Forest Using a Self-Calibration Algorithm. *Int. J. Appl. Earth Obs. Geoinf.* **2020**, *93*, 102191. [CrossRef]
78. Belgiu, M.; Drăguţ, L. Random Forest in Remote Sensing: A Review of Applications and Future Directions. *ISPRS J. Photogramm. Remote Sens.* **2016**, *114*, 24–31. [CrossRef]

79. Junttila, V.; Kauranne, T.; Finley, A.O.; Bradford, J.B. Linear Models for Airborne-Laser-Scanning-Based Operational Forest Inventory with Small Field Sample Size and Highly Correlated LiDAR Data. *IEEE Trans. Geosci. Remote Sens.* **2015**, *53*, 5600–5612. [CrossRef]
80. Grafström, A.; Ringvall, A.H. Improving Forest Field Inventories by Using Remote Sensing Data in Novel Sampling Designs. *Can. J. For. Res.* **2013**, *43*, 1015–1022. [CrossRef]
81. Saarela, S.; Schnell, S.; Grafström, A.; Tuominen, S.; Nordkvist, K.; Hyyppä, J.; Kangas, A.; Ståhl, G. Effects of Sample Size and Model Form on the Accuracy of Model-Based Estimators of Growing Stock Volume. *Can. J. For. Res.* **2015**, *45*, 1524–1534. [CrossRef]
82. Blázquez-Casado, Á.; Calama, R.; Valbuena, M.; Vergarechea, M.; Rodríguez, F. Combining Low-Density LiDAR and Satellite Images to Discriminate Species in Mixed Mediterranean Forest. *Ann. For. Sci.* **2019**, *76*, 57. [CrossRef]
83. Prieur, J.-F.; St-Onge, B.; Fournier, R.A.; Woods, M.E.; Rana, P.; Kneeshaw, D. A Comparison of Three Airborne Laser Scanner Types for Species Identification of Individual Trees. *Sensors* **2021**, *22*, 35. [CrossRef] [PubMed]
84. Zhong, H.; Zhang, Z.; Liu, H.; Wu, J.; Lin, W. Individual Tree Species Identification for Complex Coniferous and Broad-Leaved Mixed Forests Based on Deep Learning Combined with UAV LiDAR Data and RGB Images. *Forests* **2024**, *15*, 293. [CrossRef]